

COMPONENTS' AND MATERIALS' PERFORMANCE FOR ADVANCED SOLAR SUPERCRITICAL CO2 POWERPLANTS

Lifetime prediction of novel particles and improvements beyond the state of the art

Deliverable Number 2.4

WP2

Date: 09 January 2025

Deliverable type: Report

Dissemination level: Public



Deliverable 2.4 Lifetime prediction of novel particles and improvements beyond the state of the art



This project has received funding from the European Union's Horizon 2020 Research and Innovation Action (RIA) under grant agreement No. **958418.**

AUTHORS

Name	Organization
Tatu Pinomaa	VTT
Liva Freimane	VTT
Abhishek Biswas	VTT
Napat Vajragupta	VTT
Florian Sutter	DLR
Florian Wiesinger	DLR
Ana Cleia Gonzalez Alves	DLR
Gözde Alkan	DLR
Gema San Vicente	CIEMAT
Angel Morales	CIEMAT
Arantxa Fernandez Garcia	CIEMAT
Samuel Marlin	Saint-Gobain
Nassira Benameur	Saint-Gobain

DOCUMENT HISTORY

Version	Date	Change
01	09.01.2025	Initial version uploaded

ABOUT THE PROJECT

COMPASsCO₂ is a 4,5-year HORIZON2020 project started on 1.11.2020. It is led by the German Aerospace Center (DLR), with eleven additional partners from seven European countries.

COMPASsCO₂ aims to integrate CSP particle systems into highly efficient s-CO₂ Brayton power cycles for electricity production. In COMPASsCO₂, the key component for such an integration, i.e. the particle/s-CO₂ heat exchanger, will be validated in a relevant environment. To reach this goal, the consortium will produce tailored particle and alloy combinations that meet the extreme operating conditions in terms of temperature, pressure, abrasion and hot oxidation/carburization of the heat exchanger tubes and the particles moving around/across them. The proposed innovative CSP s-CO₂ Brayton cycle plants will be flexible, highly efficient, economic and 100% carbon neutral large-scale electricity producers.

The research focus of COMPASsCO2 is on three main technological improvements: development of new particles, development of new metal alloys and development of the heat exchanger section.

DISCLAIMER

This project has received funding from the European Union's Horizon 2020 Research and Innovation Action (RIA) under grant agreement No. **958418.**

The content of this publication reflects only the author's view and not necessary those of the European Commission. The Commission is not responsible for any use that may be made of the information this publication contains.

TABLE OF CONTENTS

Lis	st of Figures	5
Lis	st of Tables	6
Lis	st of Abbreviations	6
1	Abstract	6
2	Computational analysis of equilibrium phases	7
3	Particle flow and collisions in the heat exchanger section	8
4	Detailed single-Particle mechanical simulations	10
4	4.1 Mechanism of particle fragmentation	12
5	Micromechanical behavior of particles	14
6	Lifetime estimation model	15
(6.1 Comparison between state-of-the-art sintered bauxite and novel particles	18
7	CONCLUSIONS	19
8	Bibliography	21

LIST OF FIGURES

Figure 1: Overview of the modeling framework7
Figure 2: Prediction of thermodynamic equilibrium phases, where a) shows the fraction of
stable phases of primary phases as a function of temperature (T) in Kelvins, and b) shows the
stoichiometry as mole fractions, as well details about the stable phases
Figure 3: Geometry set-up for heat exchangers following CVR's Cold Test experiments 9
Figure 4: Particle flow in the heat exchanger section (left), detailed particle impact simulations
and degradation (right)9
Figure 5: Representative impact force as a function of time (top), and a cumulative time-
integrated force (bottom).
Figure 6: Workflow to simulate particle crushing tests for gen 3 and 4 particles, where a)
illustrates the geometric set-up, b) shows the experimental and simulated force vs.
displacement curves, c) shows the maximum principal logarithmic strain distribution and
displacement level 0.029 mm, and d) shows the calibrated material mechanical properties
according to the Johnson-Holmquist model for brittle materials11
Figure 7: Calibration of the temperature dependence of particle mechanical behavior for gen 3
granulated particles, with a) room temperature parametrization, b) 800 Celcius degree
parametrization. The mechanical parameters are colored according to how much they differ,
where blue indicates moderate change, and orange indicates a large change12
Figure 8: Top: compressive particle strain at different depths from surface under compression.
Bottom: evolution of particle strain distribution, where gray-red is high tensile stress state and
blue-green is high compressive state13
Figure 9: Effect of shape for particle cracking on the mechanical behavior, with a) irregularly
shaped particle, b) near-perfect sphere, and c) the corresponding force-displacement curves. 14
Figure 10: Microstructural mechanical model for sintered bauxite particles: a) scanning
electron microscopy (SEM) image of the particle microstructure, b) machine vision (ImageJ's
WEKA module) based classification of the microstructure into green i.e. Al2O3 and red i.e.
fused silica) c) the binary segmentation image, d) the confidence map, and e) an unstructured
finite element mesh conforming to the phase boundaries, using OOF2
Figure 11: Simulated tensile loading test of the particle microstructures, where a) shows a
measure of "plastic" deformation and b) shows the segmented phase distribution
Figure 12: Granulated particles with the two dominant thermodynamic phases: Fe2O3 and
SiO2 (quartz), the parametrization through experimental crushing tests, and a simulated
compression test of the microstructure
Figure 13: Single particle crushing test at Saint-Gobain for the state of the art (BL 16/30) and
the novel generation four (Gen 4) proppants: (left) scatter of particle diameter versus crushing
force raw data, (right)) radial stress profile relative to the deformation center as lines and
average tensile stress value as circles16
Figure 14: (left): average tensile stress vs. particle diameter in the Saint-Gobain crushing tests,
and (right): histogram of the corresponding breaking probability and estimated Weibull
distributions for the proppant materials17
Figure 15: Relating impact velocity to the particle mechanical response: (left) Prediction of the
maximum contact force as a function of impact velocity, and (right) the corresponding average
tensile stress in the contact17

LIST OF TABLES

LIST OF ABBREVIATIONS

COMPASsCO2	Components' and Materials' Performance for Advanced Solar Supercritical CO2 Power Plants						
CST	Concentrating Solar Thermal						
EC	European Commission						
EU	European Union						
DFI	Dechema Forschungsinstitut						
RT	Room Temperature						

1 ABSTRACT

This deliverable describes the modelling work that has been undertaken to better understand the particles and thereby assist in their design. This includes an analysis of the phase stabilities as a function of temperature, micromechanical response of individual particles including the effect of the underlying microstructure, as well as their mechanical behavior in tubular heat exchanger, thus representing realistic concentrated solar thermal (CST) application conditions. An overview of the framework is shown in Figure 1.

This document presents the findings on the mechanical performance and lifetime prediction of novel particles to be used in advanced solar supercritical CO₂ power plants. Through computational modeling and experimental testing, we examined phase stability, micromechanical behavior, and fracture mechanisms of particles under extreme conditions, including high temperatures and mechanical stresses in heat exchangers. Our analyses, supported by thermodynamic calculations and discrete element simulations, identified critical factors influencing particle durability, such as microstructure, shape, and phase composition. The results provide valuable insights into the design of particle materials that can withstand the demanding operational conditions of CST applications, potentially enabling more efficient, durable, and carbon-neutral energy solutions.

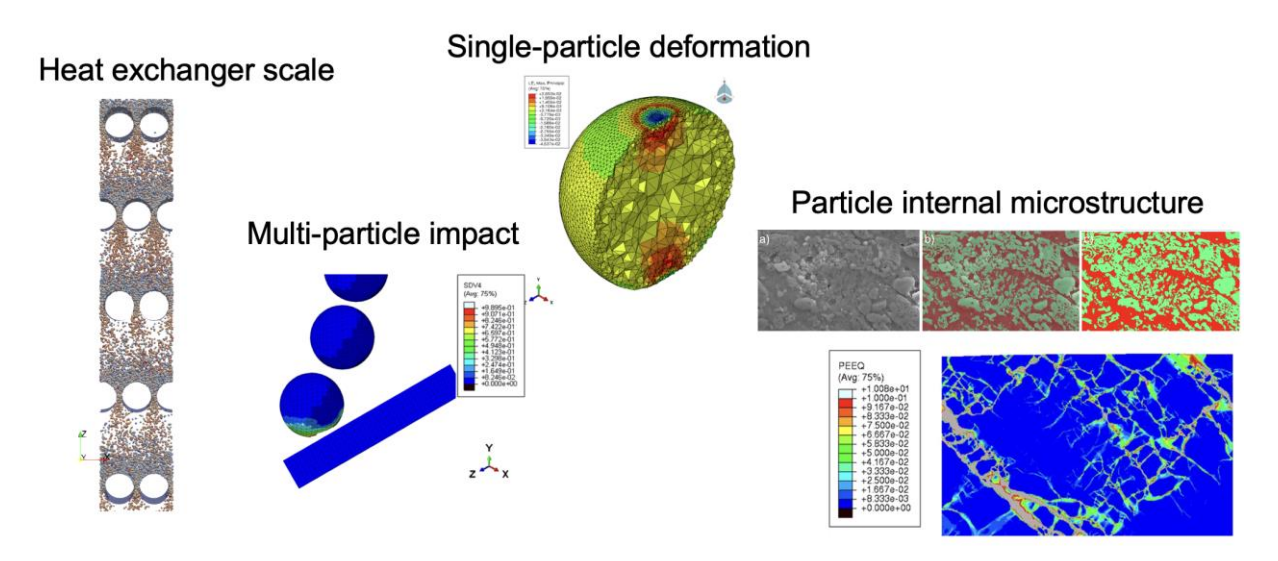


Figure 1: Overview of the modeling framework.

2 COMPUTATIONAL ANALYSIS OF EQUILIBRIUM PHASES

The mechanical properties of the CST particles are strongly tied to the present thermodynamic phases. For this purpose, we carried out computational thermodynamics calculations to predit the stable phases using Thermo-Calc and its TCOXID database, as shown in Figure 2. The primary crystalline phase is predicted to be the M2O3-type corundum phase which is mostly Al2O3, mullite-type 2M2O3-SiO2 phase which is also mostly Al2O3 with some Fe, and a pseudo-brookite phase as indicated in Figure 2 . An important feature is that the fraction of disordered or amorphous phase starts to rise around 900 °C (1173 K); the amorphous phase is known to quickly soften after a certain temperature, which can significantly influence the mechanical properties of the material.

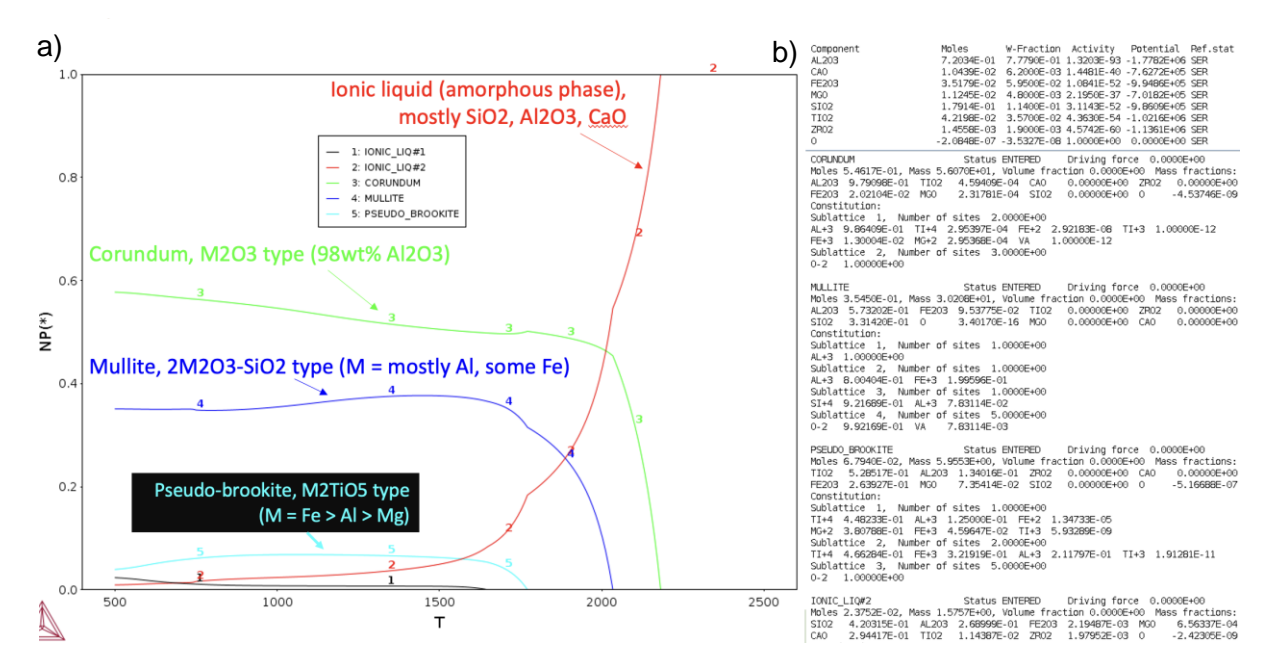


Figure 2: Prediction of thermodynamic equilibrium phases, where a) shows the fraction of stable phases of primary phases as a function of temperature (T) in Kelvins, and b) shows the stoichiometry as mole fractions, as well details about the stable phases.

3 PARTICLE FLOW AND COLLISIONS IN THE HEAT EXCHANGER SECTION

The particle impacts were simulated with a discrete element method (DEM). The arrangement of the heat exchanger tubes is specified in Figure 3, corresponding to CVR's Cold Test experiments. In the simulations, we consider two and a half vertical arrays of heat exchanger tubes, and five horizontal rows, as shown in Figure 4. The resulting particle velocities are shown, where it can be seen that the average particle velocity oscillates vertically: the particles gather speed in between the tubes, and decelerate before and around the time they meet the next vertical tube array, due to collisions with the tubes and with each other. This allows us to estimate the typical particle impact velocities when they impact each other and the heat exchanger tubes, and thereby we can estimate the mechanical loading that the particles experience, and simulate these loading conditions.

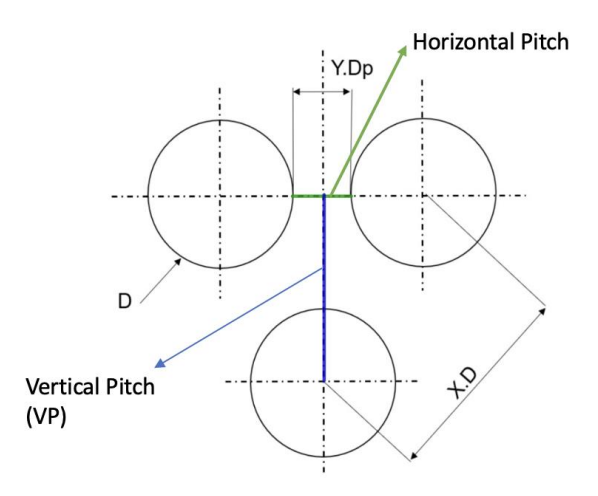


Figure 3: Geometry set-up for heat exchangers following CVR's Cold Test experiments.

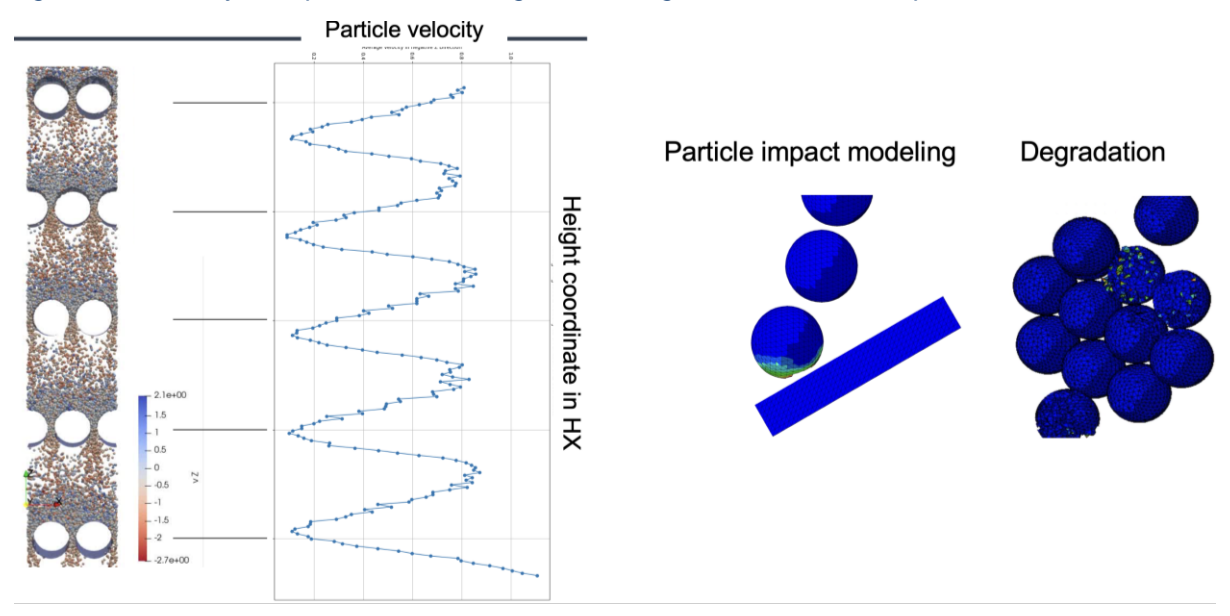


Figure 4: Particle flow in the heat exchanger section (left), detailed particle impact simulations and degradation (right).

Figure 5 shows a representative impact force over time, which has a local maximum. Also, a "cumulative" force is shown, where the force over time is integrated and will be used for comparisons. The force is calculated using a so-called Hertzian contact model, which assumes an idealized elastic interaction between a spherical (particle) surface and plane (heat exchanger tube surface). The particle material properties are those of the Granulated Gen-4 particles developed by the partner Saint-Gobain, with a density of 3600 kg/m³ and an elastic modulus of 112 GPa.

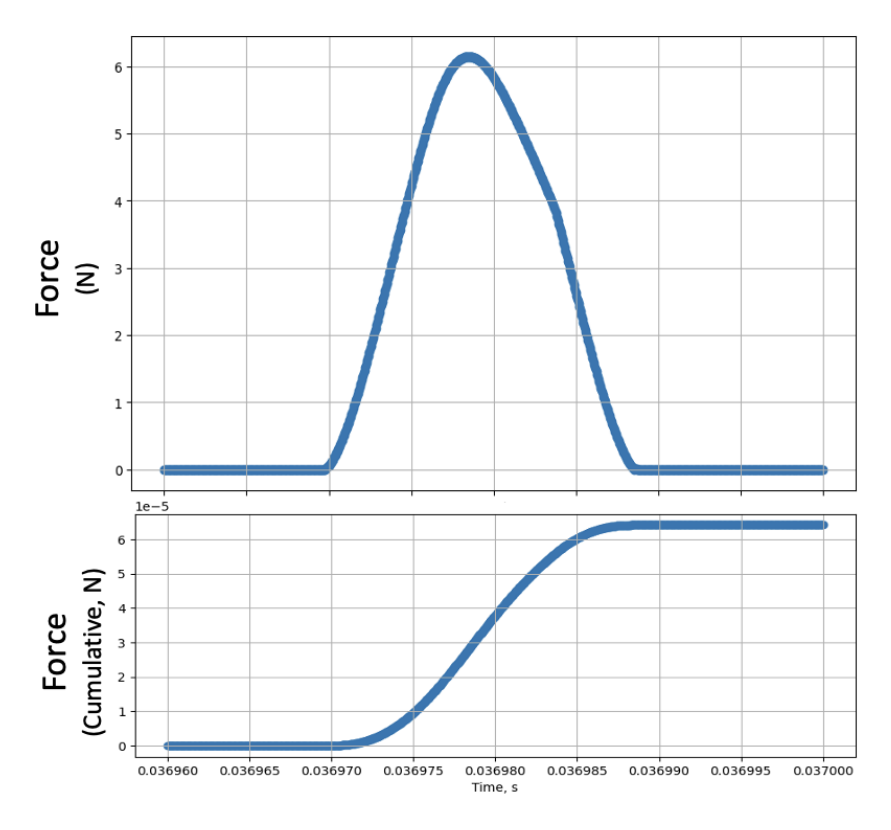


Figure 5: Representative impact force as a function of time (top), and a cumulative time-integrated force (bottom).

4 DETAILED SINGLE-PARTICLE MECHANICAL SIMULATIONS

Experimental particle crushing tests, carried out by Saint-Gobain, were used to calibrate the material mechanical model. The workflow is shown in Figure 6 for Granulated Gen-3 and Gen-4 particles, where a) illustrates the geometric set-up, b) shows the experimental and simulated force vs. displacement curves, c) shows the maximum principal logarithmic strain distribution and displacement level 0.029 mm, and d) shows the calibrated material mechanical properties according to the Johnson-Holmquist model for brittle materials. The figure shows that generation 3 particles break at lower displacement and force; the calibrated mechanical model verifies this behavior, and in Figure 6 d's material parameters tables, highlighted in yellow, shows that indeed the generation 3 particles are stiffer.

The strength of this approach is that we can systematically investigate how the materials in terms of their mechanical behavior by performing these simulations, and also we can calibrate material model parameters that are hard to acquire otherwise, which can then be used for further analyses, such as microstructure scale mechanical simulations.

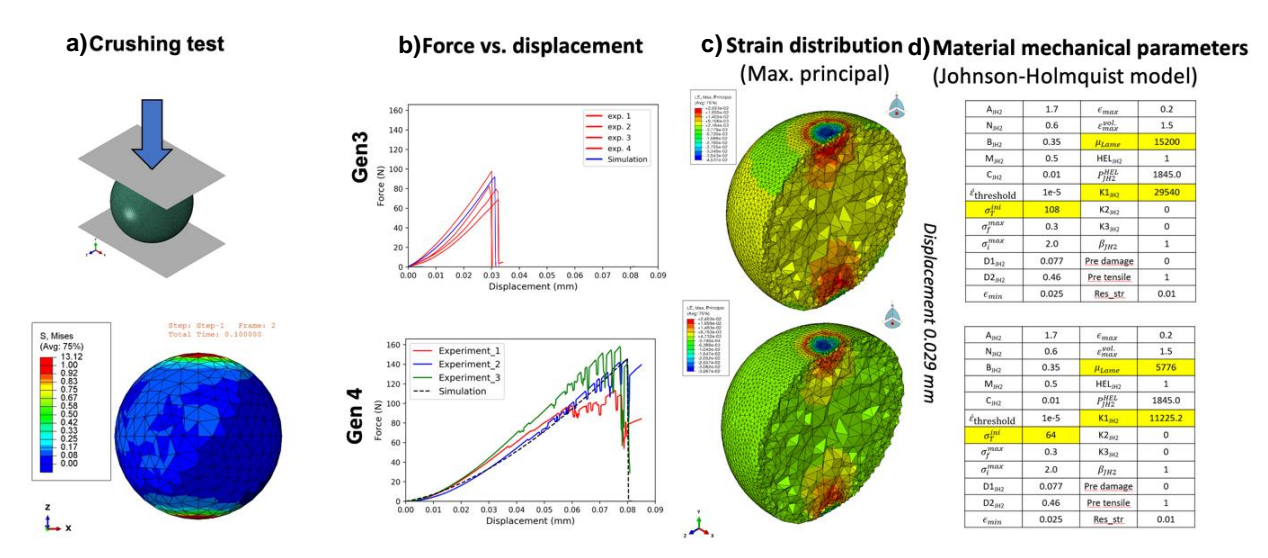


Figure 6: Workflow to simulate particle crushing tests for gen 3 and 4 particles, where a) illustrates the geometric set-up, b) shows the experimental and simulated force vs. displacement curves, c) shows the maximum principal logarithmic strain distribution and displacement level 0.029 mm, and d) shows the calibrated material mechanical properties according to the Johnson-Holmquist model for brittle materials.

The calibration of the mechanical model with respect to temperature is shown in Figure 7. It can be seen that at 800 °C, the particle fractures catastrophically much more early that at room temperature. In part, this can be explained by a thermodynamic analysis: the fraction of amorhous oxide phases increases with temperature, and the amorphous phases have a tendency to soften much more quickly than crystalline oxide phases. The change in mechanical behavior with temperature is also reflected in the Johnson-Holmquist mechanical model parameters in in Figure 7, where the changes in the Lame elastic constant and K1_{JH2} are most significant.

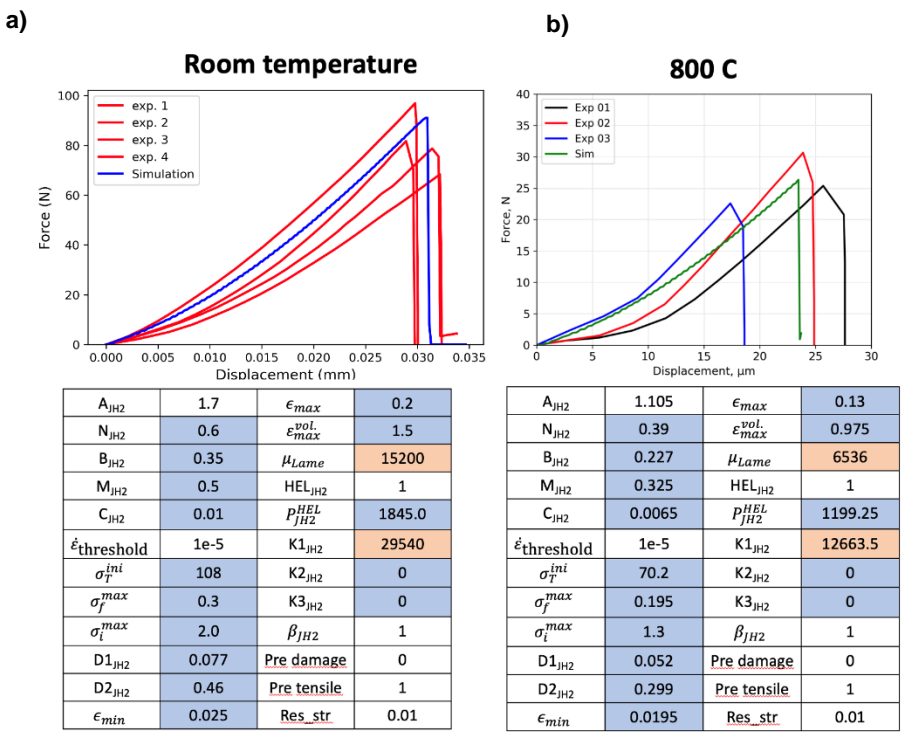


Figure 7: Calibration of the temperature dependence of particle mechanical behavior for gen 3 granulated particles, with a) room temperature parametrization, b) 800 Celcius degree parametrization. The mechanical parameters are colored according to how much they differ, where blue indicates moderate change, and orange indicates a large change.

4.1 MECHANISM OF PARTICLE FRAGMENTATION

A potential mechanism of particle fragmentation is shown in Figure 8, where compressive particle strain at different depths from surface are presented. This shows that at the surface, the strain state is mostly compressive, and subsurface strains have tensile component, which generally is more likely to initiate fracture for brittle materials. At the bottom of Figure 8, the evolution of particle strain distribution at intermediate compressive load, high compressive load, and right after the particle fracture is shown, where gray-red areas correspond to high tensile stress state and blue-green to high compressive state; this shows how the particle fracture tends to initiate at the particle subsurface.

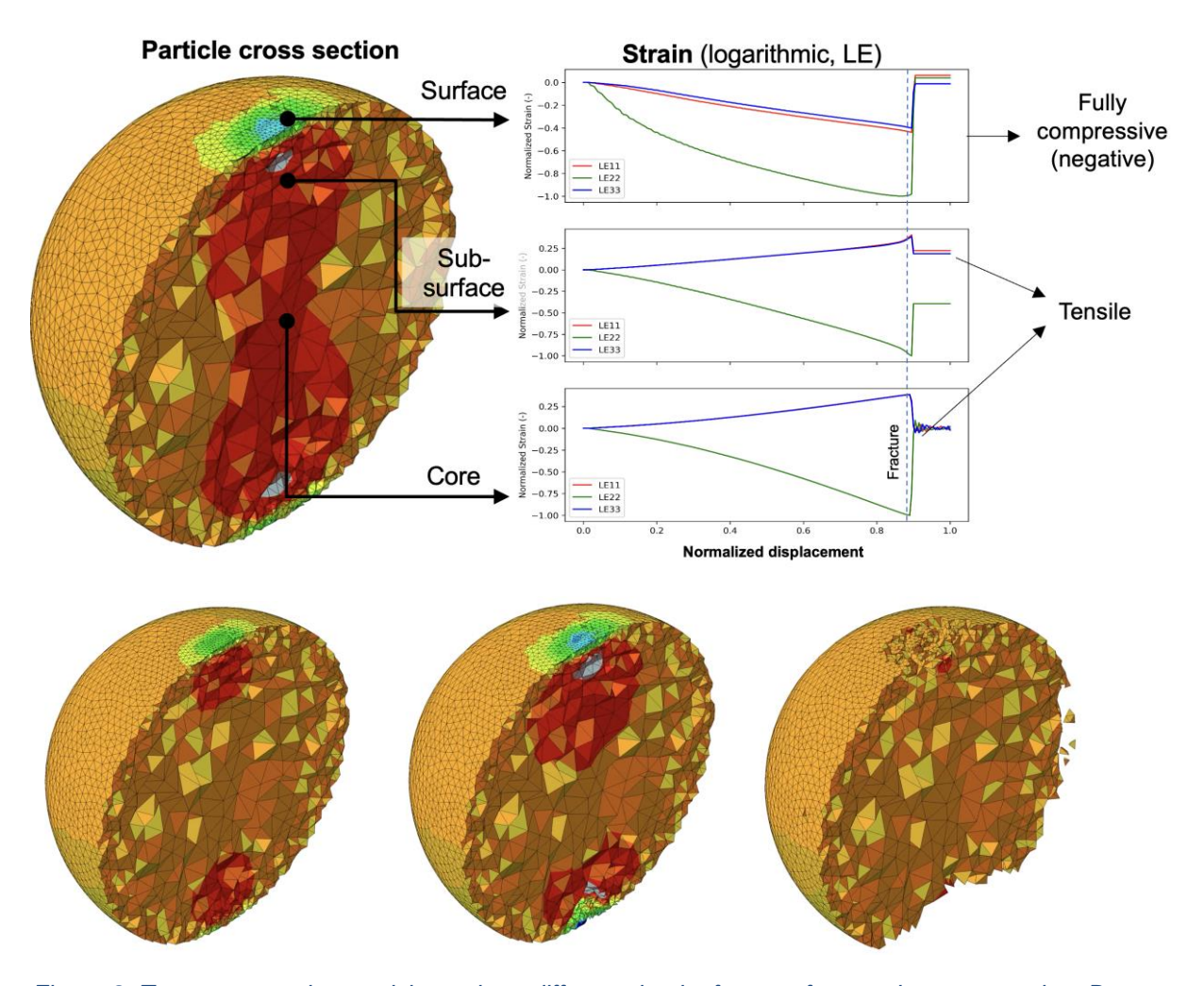


Figure 8: Top: compressive particle strain at different depths from surface under compression. Bottom: evolution of particle strain distribution, where gray-red is high tensile stress state and blue-green is high compressive state.

As acknowledged earlier, the particle shape has a significant influence on its mechanical behavior. Therefore, we compared the compression simulation of an ideal spherical particle to a highly irregular particle shape, shown in Figure 9. The stress distribution becomes highly localized early in the irregularly shaped particle, which is shown as a green circle in Figure 9 a. This leads to an early catastrophic fracture, which is visible in the full loss of structural integretiy at much lower displacement in Figure 9 c.

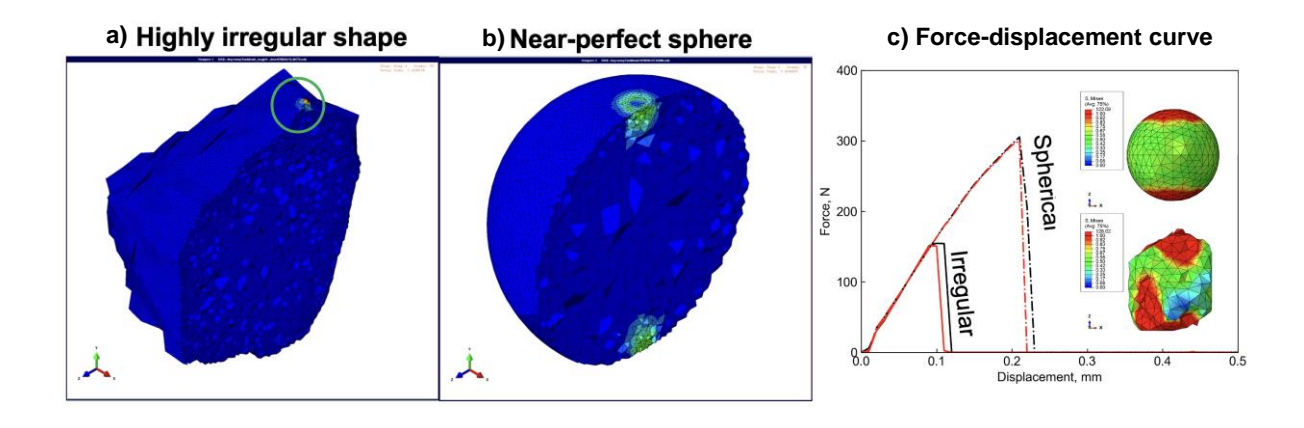


Figure 9: Effect of shape for particle cracking on the mechanical behavior, with a) irregularly shaped particle, b) near-perfect sphere, and c) the corresponding force-displacement curves.

5 MICROMECHANICAL BEHAVIOR OF PARTICLES

Based on the understanding of the dominant thermodynamic phases, a micromechanical simulation model can be developed. This work relies heavily on microstructural characterization work carried out in previous deliverables. The workflow showing the digitalization of the particle microstructure for micromechanical analysis is shown in Figure 10.

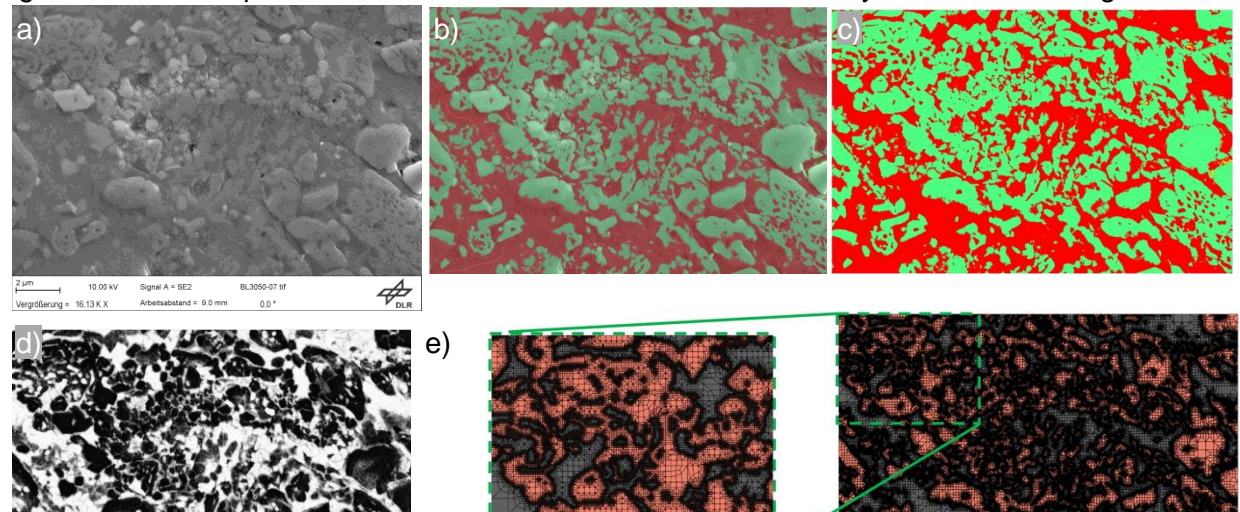


Figure 10: Microstructural mechanical model for sintered bauxite particles: a) scanning electron microscopy (SEM) image of the particle microstructure, b) machine vision (ImageJ's WEKA module) based classification of the microstructure into green i.e. Al2O3 and red i.e. fused silica) c) the binary segmentation image, d) the confidence map, and e) an unstructured finite element mesh conforming to the phase boundaries, using OOF2.

Digitalization of an experimental microstructure contains the following steps: a) scanning electron microscopy (SEM) image of the particle microstructure, b) machine vision (ImageJ's WEKA module) based classification of the microstructure into two primary phases, c) the binary segmentation image, d) the confidence map, and e) an unstructured finite element mesh conforming to the phase boundaries, using Object Oriented for Finite Elements 2D (OOF2), which is an open-source library for finite element mechanics. Mechanical properties (elastic moduli, Poissons ratios, fracture strengths) are assigned, so that green regions assumed to be Al2O3, and red regions assumed to be amorphous oxide glass (fused silica) for which good mechanical properties exist in the literature.

For the digitalized finite element mesh, a simulated tensile test is shown in Figure 11. The softer red region, i.e. fused silica, deforms more heavily, with diagonally aligned deformation bands, where shear stresses are maximized.

a) b)

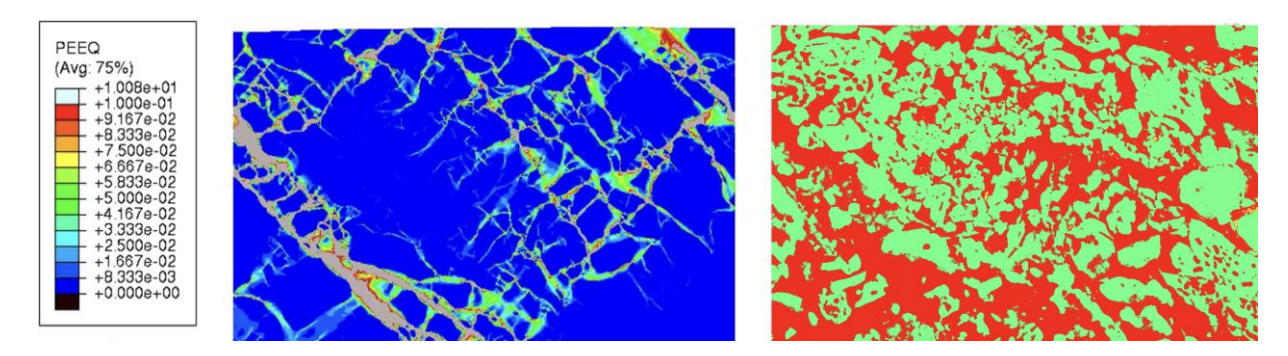


Figure 11: Simulated tensile loading test of the particle microstructures, where a) shows a measure of "plastic" deformation and b) shows the segmented phase distribution.

In a similar manner, a virtual microstructure for granulated particles was synthesized, shown in Figure 12. It can be seen that large stress peaks emerge even in a compressive state due to microstructural heterogeneities, where the harder SiO2 (quartz) particles develop high local stresses, and the softer Fe2O3 matrix goes through more deformation.

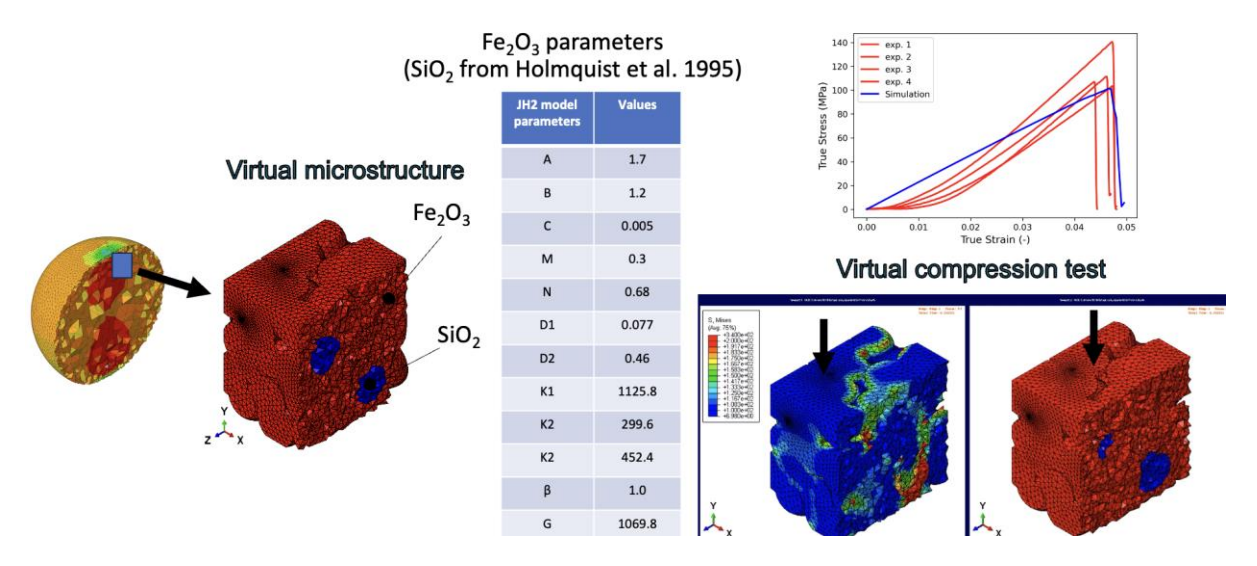


Figure 12: Granulated particles with the two dominant thermodynamic phases: Fe2O3 and SiO2 (quartz), the parametrization through experimental crushing tests, and a simulated compression test of the microstructure.

6 LIFETIME ESTIMATION MODEL

Unlike typical ductile metals, brittle materials are unable to forego plastic deformation, and therefore they tend to produce large cracks that are often catastrophic, when stressed beyond their elastic limit. These cracks initiate at stress peaks, which occur at microstructural features such as boundaries between two phases, internal pores, or material surface asperities. Because the distribution of these type of features is stochastic relative to the mechanical loading domain, the fracture initiation has a stochastic nature. Therefore, at a given loading condition, there is an inherent stochasticity and scatter in the fracture of brittle materials: sometimes very low loading levels lead to fracture, sometimes they can withstand very high

mechanical loading. A simple approach to modelling the mechanical strength of brittle materials is through a Weibull distribution. (Danzer, 1992)

The statistics of single particle crushing tests, carried out by Saint-Gobain and presented in Deliverable D2.3., are shown in Figure 13 (left), where the state-of-the-art proppant (BL 16/30) is compared to the generation four (Gen 4) particles. From the crushing force vs. particle diameter crushing test, there is no apparent correlation between particle sizes and crushing forces, and the Gen 4 and BL 16/30 particles seem to perform similarly. However, the spatial heterogeneous distribution of stresses in the particle material is what initiates the fracture, and therefore this needs to be modelled. For this purpose we use a Hertzian contact model (Johnson, 1985), which assumes an elastic contact between the particle and the surface that is used for the contact. Close to the boundary of the approximately circular deformed domain, it is known that the radial stress becomes tensile very close to the boundary of the deformed region; in brittle materials, this is evidenced by ring-shaped crack pattern around the deformation boundary (Papšík R, 2023), because brittle materials tend to initiate cracks in a tensile stress state (compressive strength in brittle materials is often an order of magnitude larger than tensile strength). For this purpose we evaluated the radial stress, and took the average of the radial stress in the domain where the radial stress is tensile. This is plotted in Figure 13 (right), revealing that upon breakage, the BL 16/30 have clearly higher maximum and average tensile stresses, latter which is indicated as circles for both materials. This suggests that the state of the art BL 16/30 proppants are able to withstand slightly local tensile stresses.

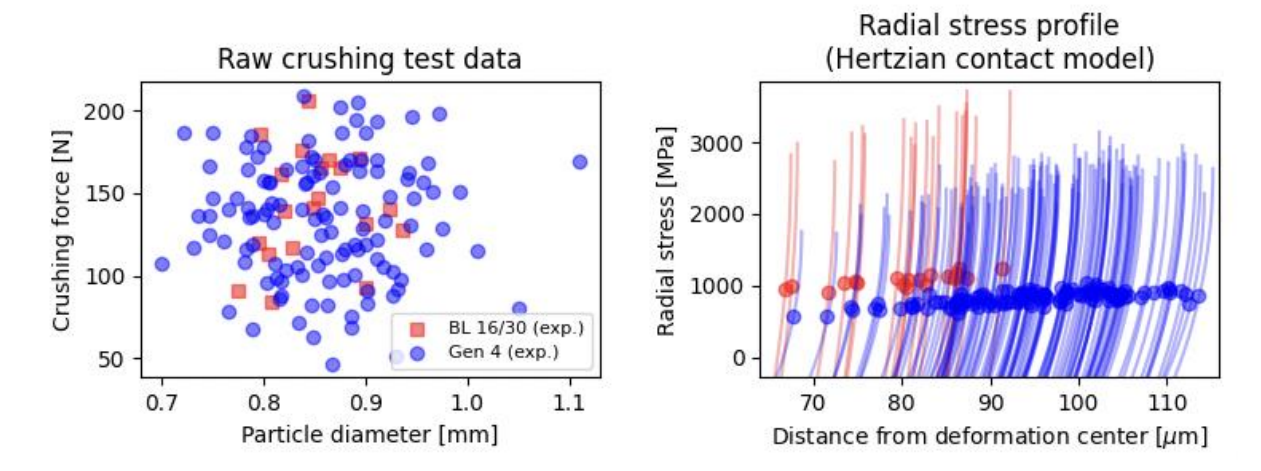


Figure 13: Single particle crushing test at Saint-Gobain for the state of the art (BL 16/30) and the novel generation four (Gen 4) proppants: (left) scatter of particle diameter versus crushing force raw data, (right)) radial stress profile relative to the deformation center as lines and average tensile stress value as circles.

As the tensile stress in the particle is a more physically motivated measure that relates to failure of brittle materials, the average tensile stress as function of the particle diameter is plotted in Figure 14 (left), where it can also be seen that there is a slight negative correlation between particle diameter and the average tensile stress. This suggests that for a given average tensile stress value, it is more likely that a larger particle will fracture, which is typical for brittle materials; it is more likely for finding a critical defect size with a sufficiently small closure stress (leading to a crack does not close but instead propagates). Due to the probabilistic nature of brittle materials, we describe the material strength as a Weibull distribution, and the experimental cumulative breaking probability histogram is shown in Figure

14 (right) together with the fitted distribution parameters. The spread of the distribution is described with the parameter k, whose value is consistent with the literature, where engineering ceramics typically have a value of approximately 10. The Gen 4 proppants also show a lower value of distribution parameter k, implying that their mechanical behavior has a lower consistency and higher scatter, and potentially more defects that are important in initiating fracture.

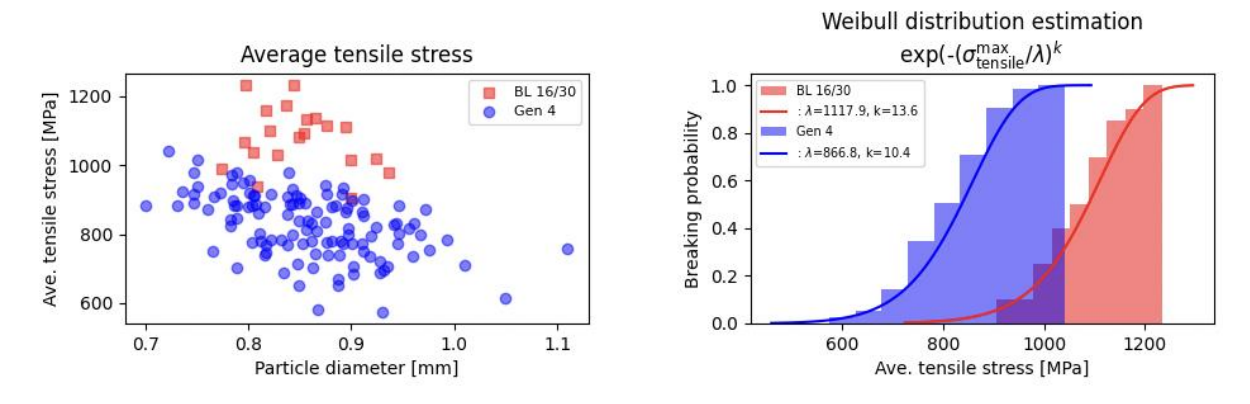


Figure 14: (left): average tensile stress vs. particle diameter in the Saint-Gobain crushing tests, and (right): histogram of the corresponding breaking probability and estimated Weibull distributions for the proppant materials.

As in CST's, the particle lifetime is limited, to a large extent, to the collisions in the solar receiver, where it is estimated that the maximum velocities are on the order of 5 m/s. For this purpose, we predict the contact mechanics as a result of the impacts, where we assume that the particle kinetic energy is transformed into elastic deformation energy and inelastic dissipation, such as plastic deformation of the impact surface. Through trial and error, we assume that only approximately 10 percent of the kinetic impact energy is transferred to elastic Hertzian contact, and we can then predict the impact force and the corresponding average Hertzian tensile stress of each impact, which are shown in Figure 15.

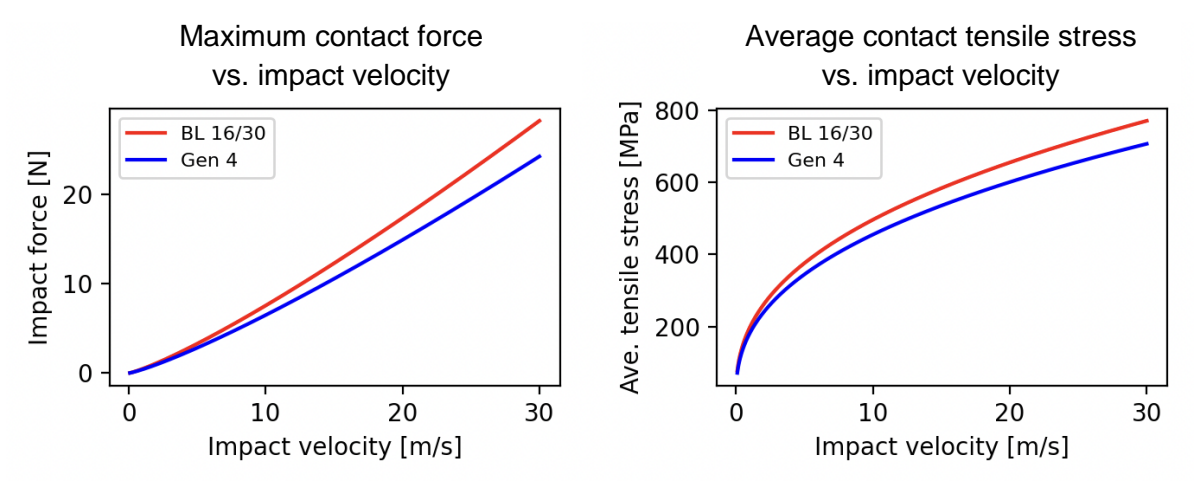


Figure 15: Relating impact velocity to the particle mechanical response: (left) Prediction of the maximum contact force as a function of impact velocity, and (right) the corresponding average tensile stress in the contact.

Then we can finally get an estimate of the breaking probability of the particles according to the fitted Weibull distribution for a single impact, shown in Figure 16. For a fixed impact velocity V, we can estimate the breaking probability after N consecutive impacts

as $1 - \left(1 - weibull(V)\right)^N$, where weibull(V) is the cumulative probability distribution of breaking at a given impact velocity. Finally, we can predict the lifetime of the particles in CST representative conditions, where it is assumed that in a year of operation, there are approximately 730 impacts with the highest velocity after leaving the solar receiver for each particle, as estimated in Deliverable 2.3, Section 5.2. Then, the ten year operation as a function of impact velocity for the two proppants can be estimated.

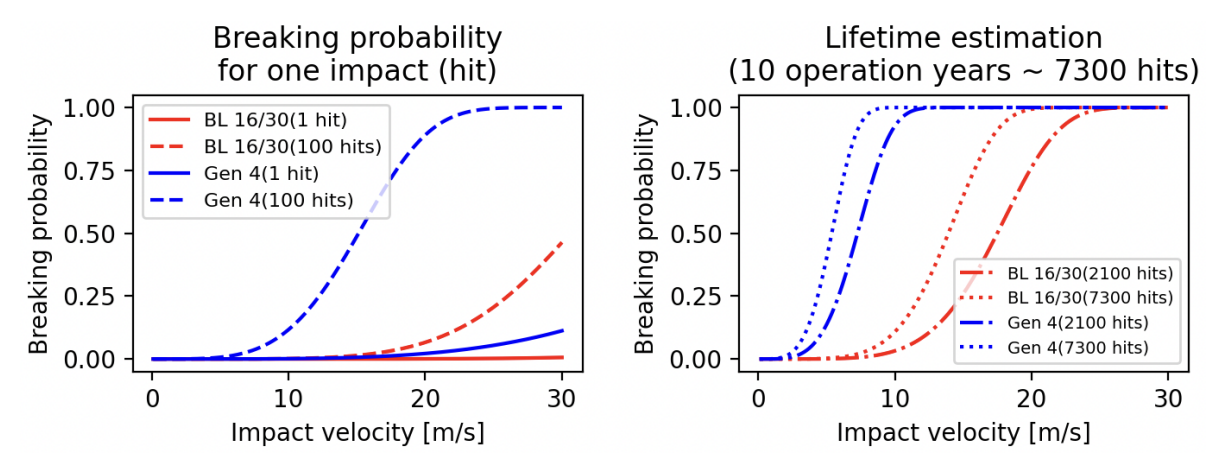


Figure 16: Lifetime estimation of for spherical particles: (left) Probability of breaking a particle in a single and 100 impacts or hits vs. impact velocity, and (right) corresponding breaking probabilities after 2100 and 7300 impacts. Ten years of operation is approximately 7300 impacts.

These results suggest that the generation four granulated particles have an overall slightly lowered lifetime compared to the state-of-the-art BL 16/30 particles. Moreover, it is interesting to point out that our mechanical modeling suggests that the generation four particles have a higher spread in the Weibull distribution that describes the particle breakage for a given tensile stress. This implies that there is likely to be more mechanically critical defects in generation four particles, which indicates a higher scatter and slightly lower consistency and reliability of the particles. However, these differences are quite small, and significantly larger experimental dataset would be needed to draw reliable conclusions. This includes a proper analysis of the roundness and smoothness of the particles versus their breaking force, which is not taken into account in the current lifetime estimation model.

6.1 COMPARISON BETWEEN STATE-OF-THE-ART SINTERED BAUXITE AND NOVEL PARTICLES MECHANICAL BEHAVIOR

As was experimentally shown in Deliverable 2.3, the novel granulated particles offer overall improved properties compared to the state-of-the-art sintered bauxite particles, as shown in Table 1. Eventhough the novel generation four particles have a lower predicted lifetime for given impact velocities, the model assumes perfectly spherical and smooth particles; in reality, the state-of-the-art particles have lower roundness, which is expected to lead to earlier break-up than anticipated by a smooth spherical particle. We explain the discrepancy between the experimentally measured mechanical properties and the lifetime predictions as follows.

As explained above, the experimental data show that the Vickers Hardness and the breaking force are generally improved compared to the state of the art. We claim that this is related to two factors. First, in the state-of-the-art particles, the softer fused silica (red areas in Figure 11b) is not forming a full continuous matrix around the harder alpha-alumina (Al2O3, green areas in Figure 11b); as the as the microstructure starts to deform, the stress cannot be

effectively communicated between the soft and hard phases, and localized deformation bands start to emerge in the soft regions, which are likely to develop stress hot spots easily, promoting early fracture. In contrast, in the novel granulated particles, the harder SiO2 quartz phase (blue in Figure 12) is better surrounded by the softer Fe2O3 matrix, in which case the system is able to act more effectively as a composite microstructure, where the softer phase is deform, but the hardness is increased by the harder quartz phase.

The second factor that can explain the improved mechanical performance of the novel particles is the improved sphericity and roundness. As shown in Figure 9 and the surrounding text, particles with large curvatures ("rough edges") promote stress hot-spots upon contact, whereas smooth boundaries distribute the load more broadly into the particle. Therefore, the larger sphericity and roundness of the novel particles are likely to mitigate stress hot-spots upon contact, and delay the on-set of fracture.

Therefore, we conclude that while the state-of-the-art sintered bauxite particles have a higher predicted lifetime, the model assumes a homogeneous perfectly smooth and spherical particles; if the microstructural details and the larger non-sphericity were taken into account, we expected that the lifetime estimation model would favor the novel generation four particles. In summary, the novel particles are expected to be highly beneficial due to their improved elevated temperature stability, lower cost, and higher roundness, when compared to the state-of-the-art particles.

Table 1: Summary of particle properties (Table 3, Deliverable 2.3), focus in the highlighted green area.

	State of the art proppants SAINT-GOBAIN				new developments SAINT-GOBAIN					
Property	Target values	Sintered Bauxite SB 30/50	BauxLite BL 16/30	BauxLite BL 30/50	InterProp IP 30/50	Fused Gen 1	Fused Gen 2	Granulated Gen 2	Granulated Gen 3	Granulated Gen 4
Size distribution [µm]		297-590	590-1190	297-590	297-590	800-1200	600-1200	600-1250	600-1200	600-1200
Cost [€/kg]	<1	1.5	<1.5	<1.5	<1.5	5	3	3	~1.3 -1.5	~1
c _p at 1000°C [J/g⋅K]	>1.1	1.28	1.16	1.11	1.07	1.20		0.88	Similar to Gen2	1.1
Bulk density ρ_b [g/cm³]	>2	1.85	1.74	1.61	1.73	2.08	2.08	2.8	2.83	2.0
Material density $ ho_m$ [g/cm³] specific /absolute	>3.5	3.3/3.45	3.06/3.42	3.12/3.26	3.16/3.34	3.47/3.53	3.32/3.39	4.71/5.07	4.92/5.04	3.56/3.76
Softening temperature T_s [°C]	>900	882	857	850	856	1110	1080	1010	1080	940
Vickers Hardness HV 0.1	>900	911	833	623	723	1110	988	636	704	926
Breaking force F [N] 0.8-1.0mm	>140		141			63	98	70	90	120-140
Sphericity [-] B/L (Q3=50.0 %)	as good as proppants	0.87	0.87	0.86	0.86	0.94	0.95	0.91	0.86	0.89
Roundness [-]	as good as proppants	0.75	0.72	0.71	0.76	0.79	0.81	0.79	0.81	0.82
Solar absorptance α [-]	>0.9	0.845	0.914	0.851	0.834	0.964	0.974	0.928	0.882	0.833
Thermal emittance ε at 900°C [-]		0.757	0.845	0.767	0.737	0.951	0.941	0.829	0.772	0.614
Degradation after 4000h at 1000°C										
Δα	<0.02	-0.156	-0.148	-0.091	-0.157	-0.030	-0.023	-0.002	+0.003	-0.012
Δε(900°C)	<0.02	-0.293	-0.305	-0.182	-0.249	-0.104	-0.086	+0.001	-0.004	-0.106

7 CONCLUSIONS

In this deliverable, the mechanical properties of the particles in terms of their microstructure, shape, and estimated lifetime was analyzed. The mechanical properties and performance of novel particle materials designed for application in advanced solar supercritical CO_2 (s- CO_2) power plants, as part of the COMPASsCO2 project, were explored. The focus was on understanding the microstructural characteristics, mechanical resilience, and lifetime estimation of these particles under extreme conditions, including high temperatures and repetitive mechanical stresses typical of concentrated solar thermal (CST) power systems.

The study employed a combination of computational thermodynamics, discrete element simulations, and experimental testing to evaluate the particles' behavior. Thermodynamic

modeling identified key phases present in the particle material at various temperatures, providing insight into how phase stability affects mechanical performance. For example, the emergence of an amorphous phase around 900°C was shown to have implications for particle softening, potentially impacting durability in prolonged high-temperature exposure. These insights underscore the need for phase stability when designing particles for high-temperature CST applications.

The discrete element modeling of particle flow within the heat exchanger section revealed that particles experience significant deceleration and acceleration as they impact the heat exchanger tubes and each other. These interactions generate mechanical stresses in the particles that, over time, contribute to particle degradation. Using the Hertzian contact model, we estimated impact forces and tensile stresses, which are key contributors to crack initiation and particle fracture in brittle materials. Such modeling is crucial for predicting the particles' lifespan, as repeated mechanical loading accelerates wear and fracture, particularly in brittle materials that lack plastic deformation mechanisms.

Detailed micromechanical simulations were conducted to assess single-particle mechanical behavior, calibrated using experimental crushing tests. Our analysis indicated that subsurface tensile stresses play a significant role in fracture initiation, especially under compressive loads where strain localizes at the subsurface. Moreover, particle shape was shown to influence fracture susceptibility, with more irregularly shaped particles exhibiting stress concentration points that increase the likelihood of cracking. These simulations highlighted the material's response to different loading conditions, and predicted that generation 4 particles have a slightly decreased mechanical strength compared to state of the art particles, where importantly, the model assumed smooth spherical particles.

Finally, lifetime estimation was conducted using a Weibull distribution to characterize the probabilistic nature of brittle material failure. The model incorporated the cumulative probability of particle fracture under repeated impacts, simulating a scenario where each particle experiences thousands of impacts over a decade-long operational period. The lifetime estimation model predicts a slightly lower lifespan of the novel particles compared to the state-of-the-art particles. We hypothesize that a critical shortcoming of this lifetime estimation model is the lack of description of roundness and surface smoothness in the analysis, which can dominate the lifetime of these particles.

Despite this, the novel particles demonstrated several advantages over the state-of-the-art sintered bauxite particles, including improved hardness, higher breaking forces, and enhanced sphericity. The microstructural analysis suggested that these improvements stem from a more effective distribution of phases within the particles. The softer Fe_2O_3 matrix in the novel particles provides a continuous structure that mitigates stress concentrations, enabling a composite-like behavior that reduces localized deformation and delays fracture onset. Additionally, the increased roundness of the novel particles reduces stress hotspots that arise during impacts, further contributing to their longevity.

In summary, the findings presented in this deliverable contribute to the development of particle materials optimized for durability and performance in CST applications. By integrating new particle compositions with enhanced microstructure and shape, the COMPASsCO2 project aims to advance the viability of s-CO2 power cycles for carbon-neutral electricity generation. Future work will focus on scaling up these results and testing the novel particles in operational environments to validate their long-term resilience and functionality in CST systems. These

advancements represent a significant step toward creating sustainable, efficient, and reliable energy solutions that meet the demands of a low-carbon future.

8 BIBLIOGRAPHY

Danzer, R. (1992). A General Strength Distribution Function for Brittle Materials. *Journal of the European Ceramic Society*, 461-472.

Johnson, K. (1985). Contact Mechanics. Cambridge University Press.

Papšík R, Š. O. (2023). Prediction of ring crack initiation in ceramics and glasses using a stress–energy fracture criterion. *Journal of the American Ceramic Society*, 4329-4342.